Representing Data as Atoms: Unifying Intra- and Inter-Sample Relationship to Discretize Data Representation

Yi-Lin Tuan¹ Zih-Yun Chiu² William Yang Wang¹

¹University of California, Santa Barbara ¹University of California, San Diego ytuan@cs.ucsb.edu zchiu@ucsd.edu william@cs.ucsb.edu

Abstract

The quality of data representation is paramount for the performance of a model. Recent research has focused on enhancing representation learning by incorporating more information about the intra-sample structures of individual data points, such as local and global attention. Additionally, researchers have explored methods to model the inter-sample relationships, including manifold, contrastive, and discrete representation learning. In this study, we introduce a new training loss, which considers both intra-sample structure and inter-sample relationships, leveraging the concept of *atoms* to represent data points. This new approach, *Atom Modeling*, offers a fresh perspective to discretize data representations within a continuous space. Through experiments, we demonstrate that Atom Modeling enhances the performance of existing models in tasks involving classification and generation, across diverse domains including vision and language. These findings underscore the potential of Atom Modeling to enhance data representation and improve model learning, suggesting a promising direction for future research.

1 Introduction

Deep learning models, such as those based on neural networks [27, 63, 66], have demonstrated success in a variety of fields, with the potential to enhance human life [2, 9, 18, 34, 36, 44, 46, 58, 67]. These models typically involve projecting raw data into a continuous representation space and then transforming this representation to produce a final prediction [37, 42]. Therefore, as [3, 39, 65], ensuring that the representations contain relevant information and minimal noise has been a major focus in deep learning research.

Recent studies have delved into developing representation learning approaches that consider the intersample relationship. For instance, Van Den Oord et al. [65] consider language and speech as inherently discrete, while images can be expressed using language [68]. To address this, their proposed vector quantization (VQ) method directly models representation in a discrete space [47, 48, 59] with a preestablished codebook, instead of a continuous space [30]. Meanwhile, Chen et al. [10], Dosovitskiy et al. [17] aim to learn representations by contrasting data features from different classes (Contrastive Learning; CL). Their loss function is well-known for the idea of pushing away negative pairs while bringing together designed, constructed positive pairs.

However, current approaches that unsupervisedly model inter-sample relationships may not fully exploit the potential advantages offered by the intra-sample structure. The intra-sample structure encompasses valuable information, such as locality and global attention, has been proven to significantly enhance model performance [1, 66]. Specifically, CL objectives [10] aim to maximize a distance metric between arbitrary paired data examples and minimize the distance for devised positive pairs. Consequently, the optimal solution heavily depends on the similarity among the positive pairs [22].

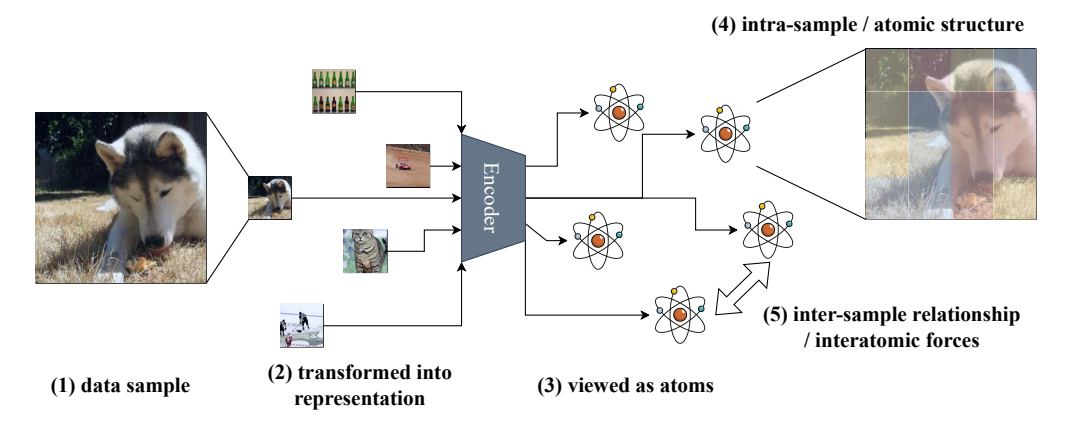


Figure 1: A sketch of atom modeling. (1) Data samples are (2) transformed into representations and (3) viewed as atoms in an *atomic space* when using atom modeling. Each data representation will learn to (4) map its intra-sample structure to an atomic structure (red: protons, blue: electrons, yellow: neutrons) and find a position in the atomic space by considering their (5) interatomic forces.

On the other hand, VQ constrains the representation using a predetermined number of codes. This approach incurs high computational costs for improved performance [19] and neglects the potential impact of the intra-sample structure. That is, the margin of the distance between arbitrary pairs in CL and VQ is not mainly determined by their intra-sample structures, potentially resulting in unbounded distance in the representation space. Hence, it is beneficial to integrate the intra-sample structure and inter-sample relationship into the training objective to address these limitations.

In this work, we present a novel approach to data representation called *Atom Modeling*. This technique unifies the intra-sample structure and inter-sample relationship within a single set of losses. Furthermore, it discretizes representations in the continuous space directly without using an additional codebook. Atom modeling is inspired by atomic physics [6, 25] and treats each data sample as an atom. As in Figure 1, it models the intra-sample structure based on atomic structure and formulates the inter-sample relationship using interatomic forces. This method has two main advantages: the optimality of the training objective for inter-sample relationships is explicitly based on the intra-sample structures (Figure 2), and the intra-

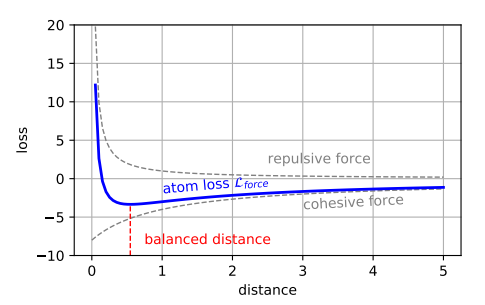


Figure 2: Proposed atom loss. The minimum, corresponding to the balanced distance, is determined by intra-sample structures.

sample structure is learned automatically without any additional supervision, leading to an enhanced data representation that also provides an interpretation as an atom.

Contrasting to recent efforts of enhancing the creation of positive pairs [21, 35] or improving downstream tasks through discrete representation [19], our focus is on the development of loss functions and model designs that maximize the distance between arbitrary pairs of examples, or in other words, discretizing representations. Our experiments demonstrate that atom modeling leads to improved results and provides interpretable, learned intra-sample structure. We hope that our work can serve as a foundation for future research in this area.

Our contributions are:

- We present a novel way of conceptualizing data as atoms, inspired by the principles of atomic physics.
- We develop a set of losses that can be used to represent neural features as atoms.
- We demonstrate the efficacy of our atomic modeling approach through both mathematical analysis and empirical experimentation.

2 Method

We introduce *Atom Modeling*, of which the key idea is to represent data points as atoms and model their atomic structures and inter-atomic forces. This method provides an unsupervised way to discretize data representations with sub-units, such as the tokens in images and texts, in neural classifiers and generative models.

2.1 Preliminary

An atom is a unit that composes molecules, crystals, metals in the nature and helps determine their properties [6, 25]. An atom is found to consist three types of subatomic particles: neutrons, protons, and electrons, where a neutron has no charge, a proton has a positive charge and is slightly lighter than a neutron, an electron has a negative charge and weigh approximately 1/1836 of a proton [49]. The structure of an atom is often described as a Bohr model [4], where the protons and neutrons form a *nucleus* that occupies a small volume of the atom; the electrons orbit around the nucleus with a *nucleus radius*.

There are two sets of forces that determine the properties and interactions of atoms: the *intra-atomic* and *inter-atomic* forces. The intra-atomic forces majorly determine the atomic structure, including the nucleus and radius. On the other side, the inter-atomic forces based on the atomic structures will highly impact the relationship among atoms. For example, they bind atoms to be a metal but avoid them having zero distances, due to the potential energy caused by the charges and atomic structures.

The fact that the inter-atomic forces will influence the relationships among atoms and are based on the atomic structure is the motivating property to represent data as atoms. We can take the intra-sample structure of a data point as the atomic structure and the inter-sample relationship has similar properties as the inter-atomic forces. This analogy introduces a new way to discretize the data points by viewing them as atoms.

2.2 Overview

As described in Figure 1, via the Atom Modeling approach, data points are first encoded into an embedding space, where each representation is viewed as an individual atom and each sub-unit of a data sample is mapped to a subatomic particles, either neutron, proton, or electron. In the meantime, the batch of representations are computed for their interatomic forces and optimized by a set of losses.

The set of losses for Atom Modeling are *loss of force* [Equation 1], *loss of charge* [Equation 2], and the *loss of particle numbers* [Equation 3]. The loss of force is derived from the Coulomb Force with the intuition that atoms will have repulsive and cohesive forces among them to prevent them from crash. This loss is the key term to discretize the representation. The loss of charge and particle numbers are empirical observation from the nature that such composition can keep an atom stable [25]. These two losses work similar as regularization.

$$\mathcal{L}_{force} = \sum_{i \sim \mathcal{A}_1, j \sim \mathcal{A}_2}^{\min(|\mathcal{A}_1|, |\mathcal{A}_2|)} \frac{q_i q_j}{d_{ij}} \qquad (Inter-Sample: Coulomb Force),$$
 (1)

$$\mathcal{L}_{charge} = \left(\sum_{i \in \mathcal{A}} q_i\right)^2 \qquad (Intra-Sample: The Charge Balance), \qquad (2)$$

$$\mathcal{L}_{p-num} = \left(\sum_{i \in \mathcal{A}} q_i^2 - \frac{2}{3}|\mathcal{A}|\right)^2 \qquad (Intra-Sample: The Numbers of Particles), \qquad (3)$$

To train a model, the set of losses are then combined with the original loss (denoted by \mathcal{L}_{ori}), for instance, mean square error or cross entropy counted towards the labels, for each task with coefficients α , β , γ as Equation 4.

$$\mathcal{L} = \mathcal{L}_{ori} + \alpha \mathcal{L}_{force} + \beta \mathcal{L}_{charge} + \gamma \mathcal{L}_{p-num}. \tag{4}$$

In the following subsections, we will introduce the derivation and detailed notations of the above equations. We will first describe the defined charge q_i of each sub-unit i in one data point A, thus

Table 1: The formulations viewing data representations as atoms. The first 5 rows: charge, mass, nucleus, nucleus radius, distance, are properties directly mapped from the original data representation $\mathbf{e_i} = [e_i^q; \mathbf{e_i^P}]$. Among them, the charge and distance are used to calculate the atom modeling losses: $\mathcal{L}_{charge}, \mathcal{L}_{p-num}, \mathcal{L}_{force}$.

Property	Our Method	Intuition [25, 49]
Charge	$q_i = 2\sigma(e_i^q) - 1$	Charge is one of $\{-1,0,+1\}$.
Mass	$m_i = 1 - \max(-q_i, 0)$	Mass of an electron $(q = -1)$ is significantly lighter than other particles.
Nucleus	$oldsymbol{\mu^P} = \sum_{i \in \mathcal{A}} \mathbf{e^P_i} m_i / A $	Nucleus consists of neutrons and protons.
Nucleus Radius	$r = \sum_{i \in \mathcal{A}} (1 - m_i) \ \mathbf{e_i^P} - \boldsymbol{\mu^P}\ _p / A $	The outermost part of an atom is composed of electrons.
Distance	$ \tilde{d} = \ \boldsymbol{\mu}_{1}^{\mathbf{p}} - \boldsymbol{\mu}_{2}^{\mathbf{p}}\ _{p} d_{ij} = \tilde{d} + \frac{r_{1} + r_{1}}{2} u(-q_{i}q_{j}) $	Our approximation written with inverse step function $u(\cdot)$.
Loss	Our Method	Intuition [25, 49]
Charge Balance	$\mathcal{L}_{charge} = \left(\sum_{i \in \mathcal{A}} q_i\right)^2$	An atom is neutral, otherwise, it is an ion.
Particle Numbers	$\mathcal{L}_{p-num} = \left(\sum_{i \in A} q_i^2 - \frac{2}{3} \mathcal{A} \right)^2$	The numbers of particles are often similar.
Interatomic Forces	$\mathcal{L}_{p-num} = \left(\sum_{i \in \mathcal{A}} q_i^2 - \frac{2}{3} \mathcal{A} \right)^2$ $\mathcal{L}_{force} = \sum_{i \sim \mathcal{A}_1, j \sim \mathcal{A}_2}^{\min(\mathcal{A}_1 , \mathcal{A}_2)} \frac{q_i q_j}{d_{ij}}$	One main force is the Coulomb Force. The caused potential is as Fig. 2.

determining their roles (neutron, proton, or electron) in the data point. Secondly, based on the roles of the sub-units and their embeddings jointly learned by the model, we formulate the atomic structure in the data representation space, in order to calculate the distance between two subatomic particles from different atoms d_{ij} . After that, we will compute their inter-atomic forces to form the set of training losses. Finally, we will discuss the properties of atom modeling that may help individuals comprehend this work and explore future directions.

2.3 The Charge of Sub-unit

Given a neural model, either a classifier or a generative model, we can extract one set of representations from one of its hidden layers. We denote the set of representations as $\{\mathbf{e}_i \in \mathbb{R}^h\}_{i=1}^N$, indicating that there are N sub-components in the data point and the embedding of each sub-component is a h-dimensional vector \mathbf{e}_i . For instance, in a transformer model or recurrent neural network, N can be the length of the input tokens, and h can be the hidden size; in a convolutional neural network, N can be the height by width of the output of a convolutional layer, and h can be the number of channels.

Without extra computational cost and loss of generality, we first split the embedding of each sub-unit into two parts $\mathbf{e_i} = [e_i^q; \mathbf{e_i^P}]$, where $e_i^q \in \mathbb{R}$ and $\mathbf{e_i^P} \in \mathbb{R}^{h-1}$. Knowing that in nature, the charge of the subatomic particles are one of -1, 0, and +1 [25], we propose a differentiable equation to compute the charge of each sub-unit by $q_i = 2\sigma(e_i^q) - 1 \in [-1,1]$, where $\sigma(\cdot)$ indicates the sigmoid function. During model training, the e_i^q for all i will be changed by the gradients from the used loss functions, and so as the charges q_i s. These charges can be interpreted to determine the roles of the sub-components in a data sample. A sub-component carries charges 0, +1, or -1 means its role is correspondingly the neutron, proton, or electron in this data sample viewed as an atom. These charges q_i and embeddings $\mathbf{e_i^P}$ for all i serve as the fundamental variables for computing the atom modeling losses.

2.4 Intra-Sample Atomic Structure

After having the charge of each sub-unit, other properties needed to compute the training losses, such as the mass, nucleus position and radius, and the distances between two particles, can be derived.

Masses (m). The empirical results in Atomic Physics [49] show that electrons have limited masses while protons and neutrons masses are in a similar level. Following these results, we approximate the mass $m \in \mathbb{R}$ of each sub-unit in a data point by $m = 1 - \max(-q, 0)$. Accordingly, the mass is about one when the charge is larger than or equal to zero (the role of the sub-unit is a proton or

neutron), and the mass will be linearly reduced to zero when the charge is negative (the role of the sub-unit is an electron). This means that when calculating the position of each atom, the positions of protons and neutrons matter the most.

Nucleus Position ($\mu^{\mathbf{P}}$). Since an atomic nucleus is composed of protons and neutrons, which occupy nearly all the mass of an atom, we approximate the position of the atomic nucleus by weighted average of the positions of the sub-units $\mathbf{e}_{\mathbf{i}}^{\mathbf{P}}$ with their masses as the weights. The position of the atomic nucleus $\mu^{\mathbf{P}} \in \mathbb{R}^{h-1}$ is thus defined as $\mu^{\mathbf{P}} = \frac{1}{|\mathcal{A}|} \sum_{i \in \mathcal{A}} \mathbf{e}_{\mathbf{i}}^{\mathbf{P}} m_i$, where $|\mathcal{A}|$ is the total number of sub-units in the data point \mathcal{A} . The derived position of the nucleus can also be interpreted as the representation of the data point in the newly defined atom space.

Nucleus Radius (r). The outermost particles of an atom are electrons, so we heuristically approximate the nucleus radius as the average distance from electrons to the nucleus. The nucleus radius $r \in \mathbb{R}$ is hence formulated as $r = \frac{1}{|\mathcal{A}|} \sum_{i \in \mathcal{A}} (1 - m_i) \|\mathbf{e}_i^{\mathbf{P}} - \boldsymbol{\mu}^{\mathbf{P}}\|_p$, where $\|\cdot\|_p$ denotes p-norm. As atomic physics where the orbited electrons often determine a large portion of an atom's property, this nucleus radius also plays an important role when determining the balanced distances between atoms.

Distances (d). Considering the geometry of an atom in a Bohr model, where the protons and neutrons form the nucleus, and electrons orbit it with a radius, we estimate the distances between a pair of particles i and j from different atoms \mathcal{A}_1 , \mathcal{A}_2 ($i \in \mathcal{A}_1$, $j \in \mathcal{A}_2$) by only μ^P and r instead of \mathbf{e}_i^P and \mathbf{e}_j^P . If $q_iq_j>0$ or say homoelectricity, we estimate the distance by $d_{ij}=\|\boldsymbol{\mu}^P_1-\boldsymbol{\mu}^P_2\|_p$. If they are heteroelectricity, i.e., $q_iq_j<0$, the distance is approximated by $d_{ij}=\|\boldsymbol{\mu}^P_1-\boldsymbol{\mu}^P_2\|_p+(r_1+r_2)/2$. The $\boldsymbol{\mu}^P$ and r subscriptted by 1 and 2 corresponds to atoms \mathcal{A}_1 and \mathcal{A}_2 respectively. These distances in the atom space, when we view the representations as atoms, are the key concept in atom modeling and are the part that we discretize, distinct from other discretizing approaches such as CL and VQ.

2.5 Inter-Sample Atomic Forces

After finding the intra-sample atomic structure in a batch, we can compute an unbiased estimation of the interatomic forces, which we adopt Coulomb Force [25], among this batch as Equation 1.

To intuitively understand how it works, one can imaging two atoms \mathcal{A}_1 and \mathcal{A}_2 are composed of different numbers of particles and each pair of particles from the two atoms have their charges and distance that constitute forces to keep them stable. These interatomic forces have two catergories: repulsive force, which pushes away two homoelectric particles, and cohesive force, which pulls closer two heteroeletric particles. The combination of the two forces, as illustrated in Figure 2, causes that the global, lowest \mathcal{L}_{force} locates at a short distance between the two data points. When their distance is close to zero, the loss increases dramatically, thus discretizing the data representations in the atom space. Moreover, the optimal of this proposed loss can be derived as follows.

Theorem 2.1. [Minimum \mathcal{L}_{force} Distance] For two atomized data examples \mathcal{A}_1 , \mathcal{A}_2 , let c_1 be the summation of q_iq_j for all homo-electric pairs and c_2 be the summation of q_iq_j for all hetero-electric pairs, $\forall i \sim \mathcal{A}_1, j \sim \mathcal{A}_2$. Assume that $c_2 = kc_1$. $\forall k > 1$, the minimum \mathcal{L}_{force} distance between \mathcal{A}_1 and \mathcal{A}_2 is equal to $\frac{\sqrt{k+1}}{k-1}c_1\frac{r_1+r_2}{2}$.

The proof, deferred to Appendix A, uses the partial derivative to find the minimum.

Theorem 2.1 implies that atomically similar data points $(k \to 1)$ result in longer balanced distance; atomically opposite data points result in shorter balanced distance, due to the partial derivative of the distance to $k, \forall k > 1$ is always negative. This theorem mathematically shows that the inter-sample relationship (the distance) is determined by the jointly learned intra-sample structures (the atomic structures and k) in our proposed atom modeling method.

2.6 Discussion

The effect of \mathcal{L}_{charge} and \mathcal{L}_{p-num} ? From the equations, \mathcal{L}_{charge} is as an regularization of the numbers of electrons and protons, to constrain there are about the same numbers. Meanwhile, \mathcal{L}_{p-num} is as a regularization of the number of neutrons, to constrain there is about 1/3 of the total number of particles in an atom. These two losses work as strong regularization to the atom space

representation, similar to the attention mechanism to bias on parts of the features. It is also notable that these constraints are essential to the assumptions of \mathcal{L}_{force} , and they are taken as a set of losses. Empirically, we set their coefficients the same ($\alpha = \beta = \gamma$ in Equation 4).

Charge and representation layer selection? We empirically test the different selections of charge and have not observed significant difference for training from scratch or fine-tuning. The experiments reported are all using the first dimension of the representation as the e_i^q . On the other hand, we treat as a hyperparameter for which hidden layer output is taken as the data representation. We have not observed a clear pattern, but empirically the nearest layer to the raw data (e.g., the first layer for classification and the last layer for generation) works well.

Gradients to the representation? In terms of differentiability, the current design of mass m_i can backpropagate the gradients to q_i for all $q_i < 0$ and stop the gradients for all $q_i > 0$. The nucleus $\boldsymbol{\mu}^{\mathbf{P}}$ can backpropagate the gradients to $\mathbf{e}_{\mathbf{i}}^{\mathbf{P}}$ for $q_i > 0$ and radius r can backpropagate the gradients to $\mathbf{e}_{\mathbf{i}}^{\mathbf{P}}$ for $q_i < 0$. All the e_i^q will receive gradients directly from all the losses. Therefore, all the parts of the representations can receive gradients. The current design is a simple mapping from atomic physics to deep learning, and other designs of properties are left for future work.

Time complexity? The complexity of \mathcal{L}_{force} is $\mathcal{O}(N^2B^2)$, where B is the batch size. To reduce the complexity, we sample only B pairs of data in each batch instead of B^2 and set a fixed number M of (i,j) for each $(\mathcal{A}_1,\mathcal{A}_2)$ pairs. The new resulting complexity is $\mathcal{O}(MB)$.

3 Related Work

There are various approaches to representation learning, including long-investigated problems such as manifold learning [8, 43, 60, 64], graph representations [23, 26, 54], and kernel tricks [31, 33, 50], which have long considered the inter-sample relationship. These approaches often already possess an assumption of the inter-sample relationship before learning and aim to find a way to better fit the learned representation into the supposed relationships. Their goals differ from our work in that we aim to discretize representation without any assumption of the inter-sample relationship. With this goal, among the many representation learning methods, VQ and CL are the most related methods to our work.

Discrete representation learning, where VQ is one of the major adopted method, has been explored in various domains such as image generation [19, 57, 65], time series [20], text generation [76], and cross-modality [45]. These approaches have been recognized for their potential to enhance interpretability [20, 45] and reduce the discrepancy between neural networks and real-world data signals [55, 65]. Typically, they involve encoding the data and subsequently compressing [65] or clustering [20] the original continuous embeddings into discrete codes.

On the other hand, CL aims to enhance the similarity among positive pairs while increasing the dissimilarity between arbitrary (negative) pairs. This approach has been developed over a considerable period, with earlier contributions including triplet [73], N-pair [62], NCE [24], and InfoNCE [52] losses. Notably, well-known models like MoCo [28] and SimCLR [10] have demonstrated the efficacy of contrastive loss in visual tasks. Recent advancements, such as SwAV [7], BYOL [22], SimSiam [11], SupCon [35], SimCSE [21], have focused on enhancing CL by proposing methods for constructing positive pairs, such as leveraging known labels or devising data augmentation techniques.

Parallel to the recent efforts in VQ and CL above, our work aims to discretize representations in a continuous space and focuses on the distance loss for arbitrary pairs of data example without particular designs. Unlike in VQ and CL, where intra-sample structures are typically only integrated into the model architecture but not considered in the training objective, our atomic modeling approach directly incorporates intra-sample structure into the inter-sample relationship loss. This fusion enhances the dynamics of the distance loss, leading to improved representation discretization. Moreover, our approach holds potential for future extensions to VQ or CL frameworks.

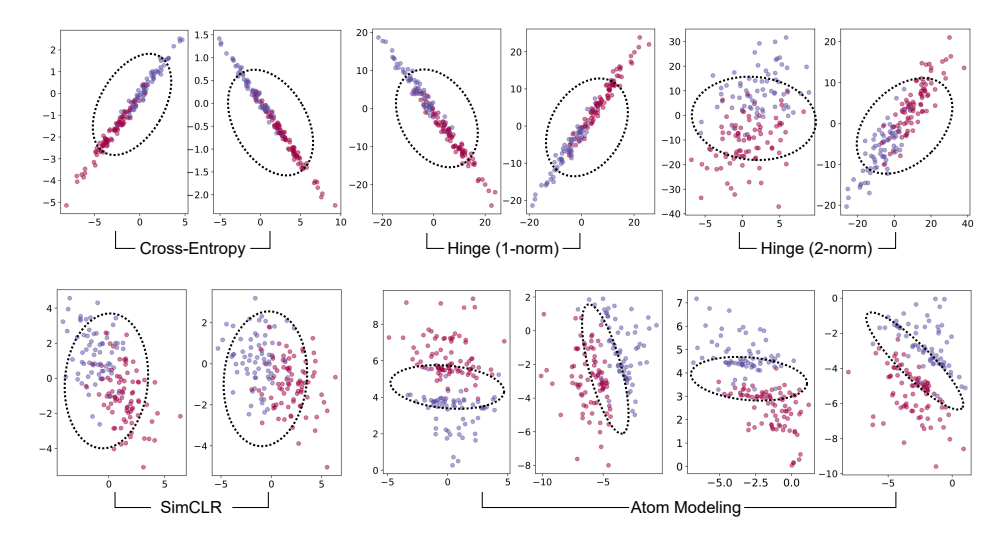


Figure 3: Visualization of the learned representations of synthetic data by only cross-entropy training loss or integrated with hinge losses (L1 and L2), SimCLR, or Atom Modeling. The dashed circles annotate the overlaps of the learned representations from different classes, which is correlated with the easiness to classify the samples. With Atom Modeling and no additional supervisions, the representations are learned to be separated with a gap.

4 Experiments

4.1 Synthetic Dataset

To demonstrate the inter-sample structure changes after discretizing representations correlated with the model prediction, we conduct experiments on synthetic data. Specifically, we generate input features X and the corresponding labels y by

$$\begin{cases}
P(A) = \mathcal{N}(\mu_a, \sigma_a) \\
P(B) = \mathcal{N}(\mu_b, \sigma_b) \\
X = \{x_i | x_i \in A \cup B\}_{i=1}^n \\
y = \mathbb{1} \left(P(x_i \in A | x_i \in X) > P(x_i \in B | x_i \in X) \right)
\end{cases} (5)$$

where A and B are two sets (events) of normal distributions with (μ_a, σ_a) and (μ_b, σ_b) to be the mean and standard deviation respectively. X is the input composed of n sub-units x_i sampled from $A \cup B$. The goal is to find a function $f: X \to y$. This synthetic data is motivated by real data such as texts and images, that are composed of multiple sub-units.

In this experiment, we use a neural network with two fully-connected linear layers and take the first layer output as the representation. For comparison, we employ Hinge loss with p-norm distances [5, 12, 41] and SimCLR [10] that uses cosine similarity as the metric on the same representation, as our baselines.

Figure 3 visualizes their learned data representations and Figure 4 shows the classification accuracy across 10 random runs. The experiment demonstrates that atom modeling, compared to other training objectives, does not equally push away arbitrary pairs of samples, but tends to spread out the representation distribution, especially the high density region. Atom modeling therefore is the only one of them that automatically creates a gap between the classes A and B in the representation space. This ability enhances the

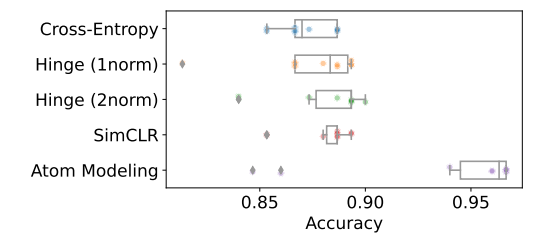
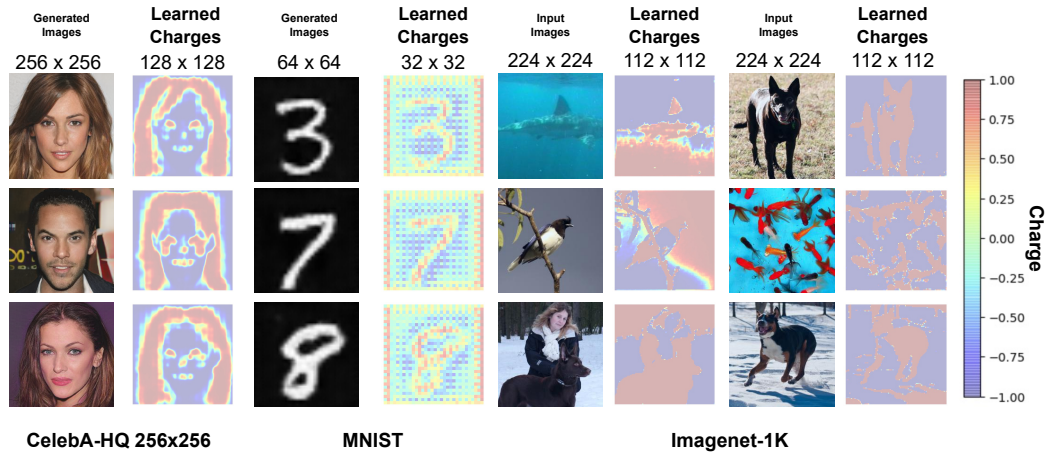


Figure 4: Comparison among cross-entropy, p-norm distance, SimCLR, and atom modeling.

classifier to achieve an average of 96% accuracy that obviously outperforms other training objectives.



Unconditional Image Synthesis

Image Classification

Figure 5: Visualization of the learned charges by atom modeling on unconditional image synthesis (CelebA-HQ 256x256, MNIST) and image classification (ImageNet-1K). The distributions show that protons (charge close to +1) are often the crucial parts in an image to be distinguished from others.

4.2 Discretizing Representations for Real World Classification Problems

For real-world data, we first validate the effects of discretizing representation with atom modeling on classification problems. It is worth noting that classification problems are already discrete in terms of labels and their theoretically well-learned representation, so it is expected that discretizing representation itself may not introduce large improvement. However, it is one of the most widely-used end tasks and worth to test the generalizability of a method.

We first experiment on fine-grained classification problems in image and text domains. Since in a fine-grained classification problem, the intra-class diversity can be higher than the interclass diversity [72], a discretizing representation approach can potentially grants much help. We select the image datasets: Oxford-IIIT Pets [53] and Oxford-Flowers102 [51], and the language datasets: CoLA [69, 71] and Poem [61] since they are often used for this testing purpose.

For comparison, we train ResNet18 [27] for image and BERT [16] for language with cross-entropy loss, while Table 2: Results of fine-grained clasemploying hinge loss with p-norm distances, Rank-H [70], SimCLR [10], SimCSE [21], and MixCSE [75]. Flowers102, CoLA, and Poem datasets.

In Table 2, we present the mean top-1 accuracy (Acc), Matthews's correlation coefficient (MCC), and F1 as used in prior work for each task. The empirical results show that our method consistently improves crossentropy as an auxiliary training objective and is the best among discretizing representation approaches.

Test on ImageNet-1K. We further examine the ability of atom modeling applied to a larger scale general classification problem on ImageNet-1K [15]. We follow prior works implementations to use ResNet50 [27] as the backbone and run 90 epochs with two data augmentation methods used in [27, 35]. The first includes only the crop and horizontal flip and the second adds color jitters and gray scale.

Table 3 show that atom modeling improves crossentropy under different data augmentations, which has been found to impact the results of image classification [13, 14, 35]. Note that this performance gain has

sification on Oxford-IIIT Pets, Oxford-

Pets	Flowers
Acc	Acc
21.0	56.7
20.0	54.7
22.4	58.0
22.4	58.2
20.7	58.1
22.5	59.1
CoLA	Poem
MCC	F1
60.0	60.3
59.8	62.0
60.1	61.8
60.8	59.3
60.4	60.8
61.3	62.7
	21.0 20.0 22.4 22.4 20.7 22.5 CoLA MCC 60.0 59.8 60.1 60.8 60.4

only been made by introducing atom modeling to one representation layer and using the exact same

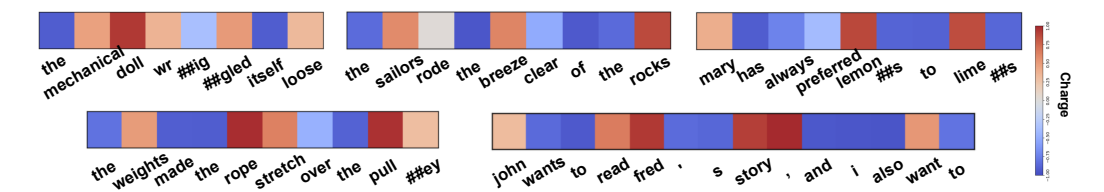


Figure 6: Visualization of the learned charges by atomic modeling on text classification (COLA). The charge distributions again show that protons are often mapped to the keywords in a sentence.

setup of conventional training of ResNet50 on ImageNet-1K; with more elaborate setting, the performance could be improved. More importantly, the outcome shows that atom modeling is generalizable to diverse classes and scales.

4.3 Unconditional Image Generation

We investigate atom modeling on generative models with unconditional image synthesis tasks: MNIST [40], CIFAR10 [38], and CelebA-HQ256x256 [32]. For MNIST and CIFAR10, we performed experiments with DCGAN [56]. For CelebA-HQ, we performed experiments with the SOTA model, StyleSwin [74], and follow their implementation.

For comparison, we employed self-supervised contrastive learning [10] and vector quantization [65] as additional loss to regularize a given representation layer and compared their ability with atom modeling for end-to-end training. In this experiment, for DCGAN, we use the output from the last hidden layer of the generator as the representation to be discretized. For StyleSwin, we use the output from the last hidden layer with half resolution. All the generated results are evaluated by Fréchet Inception Distance (FID) [29] with 2k images for MNIST, 10k for CIFAR10, and 30k for CelebA-HQ. Lower FID indicates better generation quality.

Empirically, Table 4 demonstrates the effectiveness of atom modeling. The proposed atom modeling outperforms VQ- or SSCL-enhanced DCGAN on MNIST (49.0 vs 69.4) and CIFAR10 (97.4 vs 110.4). Additionally, our approach improves StyleSwin on CelebA-HQ256x256 in our reproduced results (5.18

Table 3: Results of ImageNet-1K with [27, 35] data augmentation approaches.

Method	Top-1	Top-5
Cross-Entropy w/ [27]	74.97	92.17
Atom Modeling w/ [27]	75.10	92.25
Cross-Entropy w/ [35]	75.02	92.20
Atom Modeling w/ [35]	75.19	92.35

Table 4: FIDs of image synthetic on MNIST, CIFAR10, and CelebA-HQ256x256.

Method	Dataset	FID
DCGAN [56]	MNIST	88.4
VQ [65]	MNIST	303.9
SSCL [10]	MNIST	69.4
Atom Modeling	MNIST	49.0
DCGAN [56]	CIFAR10	110.4
VQ [65]	CIFAR10	-
SSCL [10]	CIFAR10	130.0
Atom Modeling	CIFAR10	97.4
VQGAN [19]	CelebA-HQ	10.2
StyleSwin [74]	CelebA-HQ	5.26
Atom Modeling	CelebA-HQ	5.18

vs 5.26). Note that this promising improvement is gained under the original setup of DCGAN and StyleSwin and not having extra tuning. Comparing to VQ and CL, atom modeling shows a better generalizability to different tasks. We anticipate that atom modeling will operate in more flexible setup and be applicable to more model types.

4.4 Visualization of the Learned Charges

To understand better atomic modeling, we can plot the charge distribution over image and language in Figure 5 and Figure 6. Figure 5 shows the learned charges of unconditional image synthesis and image classification. Across different tasks, the most distinguishable area of an image is often learned to be a proton. Meanwhile, the areas that surround protons and can be also used to portray the protons are learned to be electrons. The rest parts that are the least important to distinguish between arbitrary two images are often learned to be the neutrons, such as the bitmap in MNIST, untraced patterns in ImageNet and edges in CelebA-HQ and ImageNet. Similarly, in Figure 6, we observe that words with special meanings and less commonly shared among sentences are learned to be protons. The often seen words but important in forming a correct sentence are learned to be electrons. The charge distributions in both image and language indicates the protons are the parts making a data sample

different from others in the representation space. This is expected when viewing data as atoms, since the protons determine majorly the mass and charge of an atom, playing the most important role. Visualizability of the learned charge distributions exhibits the interpretability of atomic modeling.

5 Conclusion

This paper proposes atomic modeling, a science-inspired approach to discretize representation within a continuous representation space in a deep neural network. Moreover, by drawing an analogy between data and atoms, our proposed approach enables learning an interpretable intra-sample structure for each data sample. A key property of atomic modeling is that it allows for a dynamic boundary that depends on the learned structural similarity between two data examples compared to conventional distance metrics. We believe that Atomic Modeling offers a potential avenue for enhancing current neural networks, and we hope it serves as a foundation for future research that explores the implications of the discrete nature of data.

Broader Impact and Limitation

In addition to recent advancements in representation learning, we propose a novel loss function inspired by atomic physics, which aims to combine intra-sample structure and inter-sample relationships in an unsupervised manner. We introduce a method called atomic modeling, which treats data as atoms and has the potential to be applied to various modalities. We have demonstrated its effectiveness in language and vision tasks.

Moreover, atomic modeling can be considered as a new distance metric for negative pairs in contrastive learning. It can also be employed to enhance vector quantizers in discrete representation learning, although these aspects require further exploration in future research.

Furthermore, through empirical observations, we have found that in terms of image generation, the semi-supervised setting (utilizing supervised cross-entropy loss along with an additional unsupervised loss) offers more noticeable advantages compared to classification, while requiring similar computational costs.

Regarding its broader impact, the application of atomic modeling is closely associated with potential negative social consequences. For instance, the misuse of modern learning algorithms in training generative models may lead to privacy breaches and the spread of misinformation. However, these potential negative impacts can be mitigated by adopting responsible training practices for specific applications. The proposed atomic modeling, to our best observation, does not impact the potential risk.

References

- [1] Dzmitry Bahdanau, Kyunghyun Cho, and Yoshua Bengio. Neural machine translation by jointly learning to align and translate. *arXiv* preprint arXiv:1409.0473, 2014.
- [2] Mihalj Bakator and Dragica Radosav. Deep learning and medical diagnosis: A review of literature. *Multimodal Technologies and Interaction*, 2(3):47, 2018.
- [3] Yoshua Bengio, Aaron Courville, and Pascal Vincent. Representation learning: A review and new perspectives. *IEEE transactions on pattern analysis and machine intelligence*, 35(8):1798–1828, 2013.
- [4] Niels Bohr. I. on the constitution of atoms and molecules. *The London, Edinburgh, and Dublin Philosophi-* cal Magazine and Journal of Science, 26(151):1–25, 1913.
- [5] Jane Bromley, Isabelle Guyon, Yann LeCun, Eduard Säckinger, and Roopak Shah. Signature verification using a" siamese" time delay neural network. *Advances in neural information processing systems*, 6, 1993.
- [6] Theodore Lawrence Brown. Chemistry: the central science. Pearson Education, 2009.
- [7] Mathilde Caron, Ishan Misra, Julien Mairal, Priya Goyal, Piotr Bojanowski, and Armand Joulin. Unsupervised learning of visual features by contrasting cluster assignments. Advances in neural information processing systems, 33:9912–9924, 2020.

- [8] Lawrence Cayton. Algorithms for manifold learning. *Univ. of California at San Diego Tech. Rep*, 12(1-17): 1, 2005.
- [9] Hongshen Chen, Xiaorui Liu, Dawei Yin, and Jiliang Tang. A survey on dialogue systems: Recent advances and new frontiers. *Acm Sigkdd Explorations Newsletter*, 19(2):25–35, 2017.
- [10] Ting Chen, Simon Kornblith, Mohammad Norouzi, and Geoffrey Hinton. A simple framework for contrastive learning of visual representations. In *International conference on machine learning*, pages 1597–1607. PMLR, 2020.
- [11] Xinlei Chen and Kaiming He. Exploring simple siamese representation learning. In *Proceedings of the IEEE/CVF conference on computer vision and pattern recognition*, pages 15750–15758, 2021.
- [12] Sumit Chopra, Raia Hadsell, and Yann LeCun. Learning a similarity metric discriminatively, with application to face verification. In 2005 IEEE Computer Society Conference on Computer Vision and Pattern Recognition (CVPR'05), volume 1, pages 539–546. IEEE, 2005.
- [13] Ekin D Cubuk, Barret Zoph, Dandelion Mane, Vijay Vasudevan, and Quoc V Le. Autoaugment: Learning augmentation strategies from data. In *Proceedings of the IEEE/CVF conference on computer vision and* pattern recognition, pages 113–123, 2019.
- [14] Ekin D Cubuk, Barret Zoph, Jonathon Shlens, and Quoc V Le. Randaugment: Practical automated data augmentation with a reduced search space. In *Proceedings of the IEEE/CVF conference on computer vision and pattern recognition workshops*, pages 702–703, 2020.
- [15] Jia Deng, Wei Dong, Richard Socher, Li-Jia Li, Kai Li, and Li Fei-Fei. Imagenet: A large-scale hierarchical image database. In 2009 IEEE conference on computer vision and pattern recognition, pages 248–255. Ieee, 2009.
- [16] Jacob Devlin, Ming-Wei Chang, Kenton Lee, and Kristina Toutanova. Bert: Pre-training of deep bidirectional transformers for language understanding. In Proceedings of the 2019 Conference of the North American Chapter of the Association for Computational Linguistics: Human Language Technologies, Volume 1 (Long and Short Papers), pages 4171–4186, 2019.
- [17] Alexey Dosovitskiy, Jost Tobias Springenberg, Martin Riedmiller, and Thomas Brox. Discriminative unsupervised feature learning with convolutional neural networks. *Advances in neural information processing systems*, 27, 2014.
- [18] Bradley J Erickson, Panagiotis Korfiatis, Zeynettin Akkus, and Timothy L Kline. Machine learning for medical imaging. *Radiographics*, 37(2):505–515, 2017.
- [19] Patrick Esser, Robin Rombach, and Bjorn Ommer. Taming transformers for high-resolution image synthesis. In *Proceedings of the IEEE/CVF conference on computer vision and pattern recognition*, pages 12873–12883, 2021.
- [20] Vincent Fortuin, Matthias Hüser, Francesco Locatello, Heiko Strathmann, and Gunnar Rätsch. Deep self-organization: Interpretable discrete representation learning on time series. In *International Conference on Learning Representations*, 2019. URL https://openreview.net/forum?id=rygjcsR9Y7.
- [21] Tianyu Gao, Xingcheng Yao, and Danqi Chen. Simcse: Simple contrastive learning of sentence embeddings. In *Proceedings of the 2021 Conference on Empirical Methods in Natural Language Processing*, pages 6894–6910, 2021.
- [22] Jean-Bastien Grill, Florian Strub, Florent Altché, Corentin Tallec, Pierre Richemond, Elena Buchatskaya, Carl Doersch, Bernardo Avila Pires, Zhaohan Guo, Mohammad Gheshlaghi Azar, et al. Bootstrap your own latent-a new approach to self-supervised learning. Advances in neural information processing systems, 33:21271–21284, 2020.
- [23] Aditya Grover and Jure Leskovec. node2vec: Scalable feature learning for networks. In Proceedings of the 22nd ACM SIGKDD international conference on Knowledge discovery and data mining, pages 855–864, 2016.
- [24] Michael Gutmann and Aapo Hyvärinen. Noise-contrastive estimation: A new estimation principle for unnormalized statistical models. In *Proceedings of the thirteenth international conference on artificial* intelligence and statistics, pages 297–304. JMLR Workshop and Conference Proceedings, 2010.
- [25] David Halliday, Robert Resnick, and Jearl Walker. Fundamentals of physics. John Wiley & Sons, 2013.

- [26] William L Hamilton, Rex Ying, and Jure Leskovec. Representation learning on graphs: Methods and applications. arXiv preprint arXiv:1709.05584, 2017.
- [27] Kaiming He, Xiangyu Zhang, Shaoqing Ren, and Jian Sun. Deep residual learning for image recognition. In *Proceedings of the IEEE conference on computer vision and pattern recognition*, pages 770–778, 2016.
- [28] Kaiming He, Haoqi Fan, Yuxin Wu, Saining Xie, and Ross Girshick. Momentum contrast for unsupervised visual representation learning. In *Proceedings of the IEEE/CVF conference on computer vision and pattern* recognition, pages 9729–9738, 2020.
- [29] Martin Heusel, Hubert Ramsauer, Thomas Unterthiner, Bernhard Nessler, and Sepp Hochreiter. Gans trained by a two time-scale update rule converge to a local nash equilibrium. Advances in neural information processing systems, 30, 2017.
- [30] Geoffrey E Hinton and Ruslan R Salakhutdinov. Reducing the dimensionality of data with neural networks. science, 313(5786):504–507, 2006.
- [31] Thomas Hofmann, Bernhard Schölkopf, and Alexander J Smola. Kernel methods in machine learning. The annals of statistics, 36(3):1171–1220, 2008.
- [32] Tero Karras, Timo Aila, Samuli Laine, and Jaakko Lehtinen. Progressive growing of GANs for improved quality, stability, and variation. In *International Conference on Learning Representations*, 2018. URL https://openreview.net/forum?id=Hk99zCeAb.
- [33] S Sathiya Keerthi and Chih-Jen Lin. Asymptotic behaviors of support vector machines with gaussian kernel. *Neural computation*, 15(7):1667–1689, 2003.
- [34] Justin Ker, Lipo Wang, Jai Rao, and Tchoyoson Lim. Deep learning applications in medical image analysis. *Ieee Access*, 6:9375–9389, 2017.
- [35] Prannay Khosla, Piotr Teterwak, Chen Wang, Aaron Sarna, Yonglong Tian, Phillip Isola, Aaron Maschinot, Ce Liu, and Dilip Krishnan. Supervised contrastive learning. Advances in neural information processing systems, 33:18661–18673, 2020.
- [36] Igor Kononenko. Machine learning for medical diagnosis: history, state of the art and perspective. *Artificial Intelligence in medicine*, 23(1):89–109, 2001.
- [37] Simon Kornblith, Mohammad Norouzi, Honglak Lee, and Geoffrey Hinton. Similarity of neural network representations revisited. In *International Conference on Machine Learning*, pages 3519–3529. PMLR, 2019
- [38] Alex Krizhevsky, Geoffrey Hinton, et al. Learning multiple layers of features from tiny images. 2009.
- [39] Phuc H Le-Khac, Graham Healy, and Alan F Smeaton. Contrastive representation learning: A framework and review. *Ieee Access*, 8:193907–193934, 2020.
- [40] Yann LeCun, Léon Bottou, Yoshua Bengio, and Patrick Haffner. Gradient-based learning applied to document recognition. *Proceedings of the IEEE*, 86(11):2278–2324, 1998.
- [41] Yann LeCun, Sumit Chopra, Raia Hadsell, M Ranzato, and Fujie Huang. A tutorial on energy-based learning. *Predicting structured data*, 1(0), 2006.
- [42] Yann LeCun, Yoshua Bengio, and Geoffrey Hinton. Deep learning. nature, 521(7553):436–444, 2015.
- [43] Tong Lin and Hongbin Zha. Riemannian manifold learning. IEEE transactions on pattern analysis and machine intelligence, 30(5):796–809, 2008.
- [44] Geert Litjens, Thijs Kooi, Babak Ehteshami Bejnordi, Arnaud Arindra Adiyoso Setio, Francesco Ciompi, Mohsen Ghafoorian, Jeroen Awm Van Der Laak, Bram Van Ginneken, and Clara I Sánchez. A survey on deep learning in medical image analysis. *Medical image analysis*, 42:60–88, 2017.
- [45] Alex Liu, SouYoung Jin, Cheng-I Lai, Andrew Rouditchenko, Aude Oliva, and James Glass. Cross-modal discrete representation learning. In *Proceedings of the 60th Annual Meeting of the Association for Computational Linguistics (Volume 1: Long Papers)*, pages 3013–3035, 2022.
- [46] Gustavo López, Luis Quesada, and Luis A Guerrero. Alexa vs. siri vs. cortana vs. google assistant: a comparison of speech-based natural user interfaces. In *International conference on applied human factors* and ergonomics, pages 241–250. Springer, 2017.

- [47] Andriy Mnih and Karol Gregor. Neural variational inference and learning in belief networks. In *International Conference on Machine Learning*, pages 1791–1799. PMLR, 2014.
- [48] Andriy Mnih and Danilo Rezende. Variational inference for monte carlo objectives. In *International Conference on Machine Learning*, pages 2188–2196. PMLR, 2016.
- [49] Peter J Mohr, Barry N Taylor, and David B Newell. Codata recommended values of the fundamental physical constants: 2006. *Journal of Physical and Chemical Reference Data*, 80(3):633–1284, 2008.
- [50] K-R Muller, Sebastian Mika, Gunnar Ratsch, Koji Tsuda, and Bernhard Scholkopf. An introduction to kernel-based learning algorithms. *IEEE transactions on neural networks*, 12(2):181–201, 2001.
- [51] Maria-Elena Nilsback and Andrew Zisserman. Automated flower classification over a large number of classes. In 2008 Sixth Indian Conference on Computer Vision, Graphics & Image Processing, pages 722–729. IEEE, 2008.
- [52] Aaron van den Oord, Yazhe Li, and Oriol Vinyals. Representation learning with contrastive predictive coding. arXiv preprint arXiv:1807.03748, 2018.
- [53] Omkar M Parkhi, Andrea Vedaldi, Andrew Zisserman, and CV Jawahar. Cats and dogs. In 2012 IEEE conference on computer vision and pattern recognition, pages 3498–3505. IEEE, 2012.
- [54] Bryan Perozzi, Rami Al-Rfou, and Steven Skiena. Deepwalk: Online learning of social representations. In Proceedings of the 20th ACM SIGKDD international conference on Knowledge discovery and data mining, pages 701–710, 2014.
- [55] Adeel Pervez and Efstratios Gavves. Stability regularization for discrete representation learning. In International Conference on Learning Representations, 2022. URL https://openreview.net/forum? id=6tmjoym9LR6.
- [56] Alec Radford, Luke Metz, and Soumith Chintala. Unsupervised representation learning with deep convolutional generative adversarial networks. arXiv preprint arXiv:1511.06434, 2015.
- [57] Ali Razavi, Aaron Van den Oord, and Oriol Vinyals. Generating diverse high-fidelity images with vq-vae-2. Advances in neural information processing systems, 32, 2019.
- [58] Muhammad Imran Razzak, Saeeda Naz, and Ahmad Zaib. Deep learning for medical image processing: Overview, challenges and the future. Classification in BioApps, pages 323–350, 2018.
- [59] Ruslan Salakhutdinov and Geoffrey Hinton. Deep boltzmann machines. In David van Dyk and Max Welling, editors, *Proceedings of the Twelth International Conference on Artificial Intelligence and Statistics*, volume 5 of *Proceedings of Machine Learning Research*, pages 448–455, Hilton Clearwater Beach Resort, Clearwater Beach, Florida USA, 16–18 Apr 2009. PMLR. URL https://proceedings.mlr.press/v5/salakhutdinov09a.html.
- [60] Lawrence K Saul and Sam T Roweis. Think globally, fit locally: unsupervised learning of low dimensional manifolds. *Journal of machine learning research*, 4(Jun):119–155, 2003.
- [61] Emily Sheng and David C Uthus. Investigating societal biases in a poetry composition system. In Proceedings of the Second Workshop on Gender Bias in Natural Language Processing, pages 93–106, 2020.
- [62] Kihyuk Sohn. Improved deep metric learning with multi-class n-pair loss objective. *Advances in neural information processing systems*, 29, 2016.
- [63] Ilya Sutskever, Oriol Vinyals, and Quoc V Le. Sequence to sequence learning with neural networks. *Advances in neural information processing systems*, 27, 2014.
- [64] Joshua B Tenenbaum, Vin de Silva, and John C Langford. A global geometric framework for nonlinear dimensionality reduction. *science*, 290(5500):2319–2323, 2000.
- [65] Aaron Van Den Oord, Oriol Vinyals, et al. Neural discrete representation learning. *Advances in neural information processing systems*, 30, 2017.
- [66] Ashish Vaswani, Noam Shazeer, Niki Parmar, Jakob Uszkoreit, Llion Jones, Aidan N Gomez, Lukasz Kaiser, and Illia Polosukhin. Attention is all you need. In NIPS, 2017.
- [67] Oriol Vinyals and Quoc Le. A neural conversational model. arXiv preprint arXiv:1506.05869, 2015.

- [68] Oriol Vinyals, Alexander Toshev, Samy Bengio, and Dumitru Erhan. Show and tell: A neural image caption generator. In *Proceedings of the IEEE conference on computer vision and pattern recognition*, pages 3156–3164, 2015.
- [69] Alex Wang, Amanpreet Singh, Julian Michael, Felix Hill, Omer Levy, and Samuel R Bowman. Glue: A multi-task benchmark and analysis platform for natural language understanding. In *International Conference on Learning Representations*, 2018.
- [70] Xiaolong Wang and Abhinav Gupta. Unsupervised learning of visual representations using videos. In *Proceedings of the IEEE international conference on computer vision*, pages 2794–2802, 2015.
- [71] Alex Warstadt, Amanpreet Singh, and Samuel R. Bowman. Neural network acceptability judgments. Transactions of the Association for Computational Linguistics, 7:625–641, 2019. doi: 10.1162/tacl_a_00290. URL https://aclanthology.org/Q19-1040.
- [72] Xiu-Shen Wei, Jianxin Wu, and Quan Cui. Deep learning for fine-grained image analysis: A survey. arXiv preprint arXiv:1907.03069, 2019.
- [73] Kilian Q Weinberger and Lawrence K Saul. Distance metric learning for large margin nearest neighbor classification. *Journal of machine learning research*, 10(2), 2009.
- [74] Bowen Zhang, Shuyang Gu, Bo Zhang, Jianmin Bao, Dong Chen, Fang Wen, Yong Wang, and Baining Guo. Styleswin: Transformer-based gan for high-resolution image generation. In *Proceedings of the IEEE/CVF conference on computer vision and pattern recognition*, pages 11304–11314, 2022.
- [75] Yanzhao Zhang, Richong Zhang, Samuel Mensah, Xudong Liu, and Yongyi Mao. Unsupervised sentence representation via contrastive learning with mixing negatives. In *Proceedings of the AAAI Conference on Artificial Intelligence*, volume 36, pages 11730–11738, 2022.
- [76] Tiancheng Zhao, Kyusong Lee, and Maxine Eskenazi. Unsupervised discrete sentence representation learning for interpretable neural dialog generation. In Proceedings of the 56th Annual Meeting of the Association for Computational Linguistics (Volume 1: Long Papers), pages 1098–1107, 2018.

A Proof of Minimum \mathcal{L}_{force} Distance (Theorem 2.1)

We first replace the distance term in the Equation 1 with its parameterization by the nucleus position $\mu^{\mathbf{p}}$ and nucleus radius r.

$$L_{f} = \sum_{i \in \mathcal{A}_{1}, i \in \mathcal{A}_{2}}^{\mathcal{A}_{1}, A_{2}} \frac{q_{i}q_{j}}{d_{ij}}$$

$$= \sum_{q_{i}q_{j} > 0} \frac{q_{i}q_{j}}{\|\boldsymbol{\mu}_{1}^{\mathbf{p}} - \boldsymbol{\mu}_{2}^{\mathbf{p}}\|_{p}} + \sum_{q_{i}q_{j} < 0} \frac{q_{i}q_{j}}{\|\boldsymbol{\mu}_{1}^{\mathbf{p}} - \boldsymbol{\mu}_{2}^{\mathbf{p}}\|_{p} + \frac{r_{1} + r_{2}}{2}}$$
(6)

To derive an equilibrium status of the loss, we first simplify the notation by defining $d \triangleq \|\boldsymbol{\mu}_{\mathbf{1}}^{\mathbf{P}} - \boldsymbol{\mu}_{\mathbf{2}}^{\mathbf{P}}\|_{p}$ and $\tilde{r} \triangleq \frac{r_{1} + r_{2}}{2}$.

$$\frac{\partial L_f}{\partial d} = \frac{\sum_{q_i q_j > 0} -q_i q_j (d+\tilde{r})^2 + \sum_{q_i q_j < 0} -q_i q_j d^2}{d^2 (d+\tilde{r})^2} = 0 \tag{7}$$

We further group two concepts by setting $c_1 \triangleq \sum_{q_i q_j > 0} q_i q_j$ and $c_2 \triangleq \sum_{q_i q_j < 0} -q_i q_j$, where c_1 indicates the total charges multiplication when two are homocharges, and c_2 indicates the total negative charges multiplication when two are heterocharges.

$$\sum_{q_i q_j > 0} -q_i q_j (d + \tilde{r})^2 + \sum_{q_i q_j < 0} -q_i q_j d^2$$

$$= (-c_1 + c_2) d^2 - 2c_1 d\tilde{r} - c_1 \tilde{r}^2$$

$$= (-c_1 + c_2) (d - \frac{c_1 \tilde{r}}{-c_1 + c_2})^2 - (-c_1 + c_2) (\frac{c_1 \tilde{r}}{-c_1 + c_2})^2 - c_1 \tilde{r}^2 = 0$$
(8)

This equation can be reduced to:

$$\left(d - \frac{c_1 \tilde{r}}{-c_1 + c_2}\right)^2 = \frac{c_1^2 + c_1(-c_1 + c_2)}{(-c_1 + c_2)^2} \tilde{r}^2 = \frac{c_1 c_2}{(-c_1 + c_2)^2} \tilde{r}^2 \tag{9}$$

Therefore, we can find a closed-form solution of d:

$$d = \left(\frac{c_1}{-c_1 + c_2} \pm \sqrt{\frac{c_1 c_2}{(-c_1 + c_2)^2}}\right) \tilde{r}$$
 (10)

To this end, we can observe two unsatisfying cases from the derived formulation of d.

- If $c_1 = c_2$, the right hand side divided by zero is undefined.
- If $c_1 > c_2$ and recall that $d = \|\cdot\|_p \ge 0$, then $\frac{c_1}{c_1 c_2} \le \sqrt{\frac{c_1 c_2}{(-c_1 + c_2)^2}}$. This results in $c_1^2 < c_1 c_2$, contradict to the premise $c_1 > c_2$.

The formulation turns out to be satisfied if and only if $c_1 < c_2$. A balance point exists in $d^* = \frac{c_1 + \sqrt{c_1 c_2}}{c_2 - c_1} \tilde{r}$.

Suppose that $c_2 = kc_1$ with k > 1, then,

$$d^* = \frac{c_1 + \sqrt{c_1 c_2}}{c_2 - c_1} \tilde{r}$$

$$= \frac{c_1 + \sqrt{kc_1}}{(k-1)c_1} \tilde{r} = \frac{\sqrt{k} + 1}{k-1} c_1 \frac{r_1 + r_2}{2}$$
(11)

This mathematical result indicates that optimizing the loss \mathcal{L}_{force} is directly related the learned atomic structures of the data samples, which are c_1 , c_2 , k in this case.

Moreover, the balanced distance d^* monotonically decreasing with respect to k. This statement can be proved by the partial derivative is less than zero $\forall k > 1$:

$$\nabla_k \frac{\sqrt{k+1}}{k-1} = -\frac{1}{2} - \sqrt{k} - \frac{1}{2}k < 0, \forall k > 1$$
 (12)

B Experimental Details

B.1 Computation

There are four types of computation usages in this work: (1) The synthetic dataset experiments were using 1 RTX2070 with Max-Q with 8G capacity. (2) The experiments of Pets, Flowers, CoLA, Poem, MNIST, CIFAR10 were using 1 Titan RTX with 24G capacity. (3) Each experiment of ImageNet-1K was using 4 Titan RTX for two days. (4) Each experiment of CelebA-HQ was using 6 Titan RTX for one week.

B.2 Used Models, Baselines, and Codes

All implementations in this work are based on PyTorch https://pytorch.org/. (1) The synthetic dataset experiments are implemented our own. (2) The experiments of CoLA and Poem are our implementation. (3) The experiments of Pets and Flowers are revised from https://github.com/kuangliu/pytorch-cifar and https://github.com/Skuldur/Oxford-IIIT-Pets-Pytorch. (4) The experiments of image generation of MNIST and CIFAR10 use exact the same script as https://github.com/pytorch/examples/tree/main/dcgan. (5) The experiments of ImageNet-1K use exact the same script as https://github.com/pytorch/examples/tree/main/imagenet. (6) The experiments of CelebA-HQ use exact the same script as https://github.com/microsoft/StyleSwin.

Our hyperparameter search is limited to the computation we have for this work and is as follows: (1) The synthetic dataset experiment: We first search the best learning rate using only cross-entropy. Secondly, we use the same learning rate for all auxiliary losses and search their coefficients in {0.5,0.2,0.1,0.05,0.02,0.01,0.005}. (2) The experiments of Pets, Flowers, CoLA, and Poem: We first search the best learning rate using only cross-entropy. Secondly, we use the same learning rate for all auxiliary losses and search their coefficients in {0.05,0.02,0.01,0.005,0.002,0.001}. (3) The experiments of ImageNet-1K, MNIST, CIFAR10, and CelebA-HQ only use the coefficient 0.02 for atom modeling without further trials.

We summarize the baselines with their math forms or the implementation details in the following, where h_i denotes the concatenation of all sub-units representations in the i-th data sample:

- Hinge (1-norm): $\mathcal{L}_i = \sum_{i=1}^N \max \left\{ 0, \|h_i, h_i^+\|_1 \|h_i, h_i^-\|_1 \right\}$.
- Hinge (2-norm): $\mathcal{L}_i = \sum_{i=1}^N \max \{0, ||h_i, h_i^+||_2 ||h_i, h_i^-||_2\}.$
- Rank-H [70]: $\mathcal{L}_i = \sum_{i=1}^N \max \left\{ 0, sim(h_i, h_i^+) sim(h_i, h_i^-) + M \right\}, M = 0.5.$
- SimCLR [10]: $\mathcal{L}_{i,j} = -\log \frac{exp(sim(h_i,h_j)/\tau)}{\sum_{k=1}^{k} \frac{1}{k\neq i)} exp(sim(h_i,h_k)/\tau)}$, where (h_i,h_j) s are positive pairs (j) being one data augmentation result of the i-th sample) and (h_i,h_k) s are all other possible pairs.
- SimCSE [21]: $\mathcal{L}_{i,j} = -\log \frac{exp(sim(h_i,h_j^+)/ au)}{\sum_{j=1}^N exp(sim(h_i,h_j^+)/ au)}$, where the h^+ is the representation produced by the same model using dropout, but at different time.
- MixCSE [75]: improved SimCSE by the modified loss $\mathcal{L}_{i,j} = -\log \frac{exp(h_i^T, h_i')}{C + \sum_{j=1}^N exp(h_i^T, SG(h_{ij}'))}$, where $C = exp(h_i^T h_i'/\tau) + \sum_j^N exp(h_i^T h_j')$, $h_{ij}' = \frac{\lambda h_i' + (1-\lambda)h_j'}{\|\lambda h_i' + (1-\lambda)h_i'\|_2}$.
- $\bullet \ \ VQ+DCGAN: the \ quantizer \ [65] \ is \ implemented \ as \ \texttt{https://github.com/MishaLaskin/vqvae}.$
- SSCL+DCGAN: revised SimCLR loss since no other positive pairs except for the sample itself exist in image synthesis $\mathcal{L}_i = -\log \frac{exp(sim(h_i,h_i)/\tau)}{\sum_{k=1}^N exp(sim(h_i,h_k)/\tau)}$.

C More Experiments

C.1 Necessity of L_{force} , L_{charge} , and L_{p-num}

We studied the impacts of the losses of force, charge, and particle numbers by investigating the results of (1) only using L_{force} , (2) using L_{force} and L_{charge} , and (3) using L_{force} and L_{p-num} .

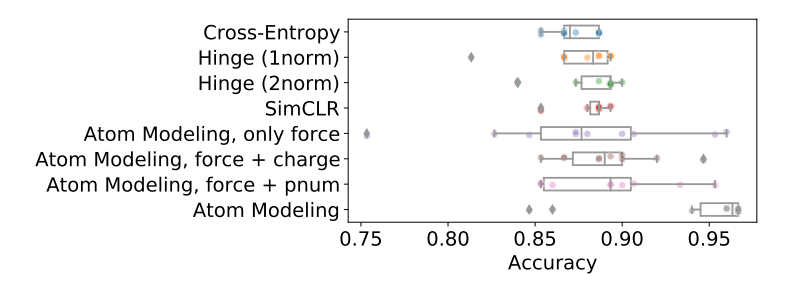


Figure 7: Ten random run results on synthetic data using only parts of Atom Modeling losses.

	MNIST		CIFAR10	
	best	average	best	average
L_{force}	-7.6	-29.4	-11.2	-16.5
$L_{force} + L_{charge}$	-25.2	-35.3	-21.4	-10.9
$L_{force} + L_{p-num}$	-2.6	-37.3	-19.9	-15.5

Table 5: The decay of FID on MNIST and CIFAR10 image synthesis with 5 random runs using only parts of the Atom Modeling losses.

From Figure 7 and Table 5, we observe that only using L_{force} in most cases can get a higher chance to achieve a better performance, but also has a higher variance and lower average scores. When adding either the L_{charge} or the L_{pnum} , the training performance is better stabilized. Using all the three proposed losses together can achieve the overall best result. In short, all the three losses are essential as our discussion in subsection 2.6. Among them, L_{force} is seen as the key component to discretize representation, while L_{charge} and L_{p-num} are acting as regularization to ensure the representation is in the atom space.

C.2 Training Time Analysis

Observed from the loss functions, the training time of Atom Modeling is dominated by L_{force} . As discussed in Section 2.6, the time complexity of L_{force} is $\mathcal{O}(MB)$, where M is the used sub-units in each data and B is the used number of data pairs. When setting the B is the batch size and M is the maximum of 100 and the data size, the average training time per iteration is listed in Table 6. The results show that Atom Modeling adds around 3-12% training time to the conventional methods and it highly depends on the difference between the set M and the data size.

	ImageNet-1K classification	MNIST synthesis
Cross-Entropy	0.665	n/a
DCGAN	n/a	0.024
Atom Modeling	0.687	0.027
Time Increased	3.3%	12.5%

Table 6: Training time (seconds) per iteration on ImageNet-1K classification and MNIST image synthesis.

C.3 Significance Test Results

The results of significance tests of Table 2 are as the following Table 7. The difference is considered significant when p-value < 0.05 and no effect when p-value > 0.1 [77].

Method vs Cross-Entropy	Pets	Flowers	CoLA	Poem
Hinge (1-norm)	0.24	0.15	0.31	0.08
Hinge (2-norm)	<u>0.09</u>	0.19	0.43	0.14
Rank-H/SimCSE	0.12	0.03	0.13	0.22
SimCLR/MixCSE	0.39	0.09	0.32	0.24
Atom Modeling	0.03	$\overline{0.02}$	0.01	0.09

Table 7: The p-value of results comparing each method to only using cross-entropy for training.

Reference

[77] Tukur Dahiru. P-value, a true test of statistical significance? a cautionary note. *Annals of Ibadan postgraduate medicine*, 6(1):21–26, 2008.